

Behavior of Self-Centering Steel Plate Shear Walls and Design Considerations

Daniel M. Dowden, P.E., S.E.¹; Ronny Purba, S.M.ASCE²; and Michel Bruneau, F.ASCE³

Abstract: This paper presents insights on the combined contribution of posttensioning and beam-to-column joint rocking connection in self-centering steel plate shear walls (SC-SPSWs). Moment, shear, and axial force diagrams along the boundary beam are developed based on capacity design principles and are compared with nonlinear cyclic push-over analysis results. These closed-form solutions are integrated into a design procedure to select cross-sectional areas of the posttension reinforcement and beam sizes: (1) to prevent in-span plastic hinges; (2) to ensure that posttension reinforcement remains elastic to maintain self-centering capability of the system; (3) to impose sufficient initial posttensioning to overcome wind and gravity loads; (4) to provide adequate beam plastic strength considering reduced moment capacity due to the presence of axial and shear forces; and (5) to consider posttension losses due to axial beam shortening. Using this fundamental behavior knowledge, and adding response-based performance objectives to the design procedure, a companion paper investigates the seismic response of SC-SPSW using time-history nonlinear analyses. DOI: 10.1061/(ASCE)ST.1943-541X.0000424. © 2012 American Society of Civil Engineers.

CE Database subject headings: Connections; Steel plates; Shear walls; Earthquake engineering; Structural design.

Author keywords: Self-centering; Rocking connection; Steel plate; Shear wall; Earthquake engineering.

Introduction

Steel plate shear wall (SPSW) systems are frames having steel plates (also known as webs) connected between their beams and columns. SPSWs have been implemented in many buildings to provide ductile seismic resistance (Sabelli and Bruneau 2007), and their design is addressed by design specifications and standards [e.g., American Institute of Steel Construction (AISC) 2005; Canadian Standards Association (CSA) 2009]. A comprehensive review of existing research on SPSW and of their advantages compared to alternate lateral force-resisting systems (LFRSs) is available elsewhere (Sabelli and Bruneau 2007). During severe earthquakes, the unstiffened plates of SPSWs buckle in shear and yield by developing a diagonal tension field, together with plastic hinging of the beams at their ends. Whereas SPSW systems are desirable for their significant stiffness, strength, and energy dissipation, the hysteretic energy dissipation of this system, like other traditional LFRSs that inherently rely on yielding of steel, results in some level of structural damage and the likelihood of significant residual drifts of the structure after severe earthquakes. As such, strategies to eliminate residual drifts and to localize structural damage only in easily replaceable structural elements are desirable in SPSWs (as in other systems).

In moment-resisting frames, use of posttension (PT) rocking moment connections was investigated to provide frame self-centering capability and to limit hysteretic damage to replaceable energy dissipating elements during earthquakes (e.g., Ricles et al. 2002; Christopoulos et al. 2002a, b; Garlock et al. 2005; Rojas et al. 2005; to name a few). Validation of performance for systems having this alternative type of moment-resisting frame connection has been established based on analytical and experimental research and shows that these types of systems could be a viable alternative to conventional LFRSs.

Building on this idea, this paper, along with a companion paper (Clayton et al. 2012), investigates the potential of achieving self-centering steel plate shear walls (SC-SPSWs) by using similar post-tensioned rocking beam connections. In this proposed system, the SC-SPSW web plate is the replaceable energy dissipation element, and beam-plastic hinging is eliminated. The system combines the advantages of high lateral stiffness, a substantial energy dissipation capacity, and self-centering capability, at the expense of additional challenges to understanding the flow of forces within the structure compared to conventional SPSWs (themselves more complex than moment frames). A fundamental understanding of behavior and of how to calculate demands on the beams of SC-SPSWs is imperative to achieve effective designs. Detailed free-body diagrams (FBDs) are essential and instructive in providing key insights for beam and system design. It is the objective of this paper to provide such insights on beam and system fundamental behavior, through free-body diagrams of individual beams, and push-over analysis of simple frames.

The focus of this paper is, first, to provide insight on the demands on beams [also known as horizontal boundary element (HBE) in SPSWs] in SC-SPSWs relying on PT moment connection rocking about the HBE flanges. Equations for the moment, shear, and axial force diagrams along the HBE are obtained from a capacity design approach based on yielding of the SPSW web plate, showing the respective contribution of each component to the total demand. Second, the insight from these closed-form solutions are

¹Graduate Research Assistant, Dept. of CSEE, Univ. at Buffalo, Amherst, NY 14260 (corresponding author). E-mail: dmdowden@buffalo.edu

²Graduate Research Assistant, Dept. of CSEE, Univ. at Buffalo, Amherst, NY 14260. E-mail: rpurba@buffalo.edu

³Professor, Dept. of CSEE, Univ. at Buffalo, Amherst, NY 14260. E-mail: bruneau@buffalo.edu

Note. This manuscript was submitted on December 14, 2010; approved on April 18, 2011; published online on December 15, 2011. Discussion period open until June 1, 2012; separate discussions must be submitted for individual papers. This paper is part of the *Journal of Structural Engineering*, Vol. 138, No. 1, January 1, 2012. ©ASCE, ISSN 0733-9445/2012/1-11-21/\$25.00.

then integrated into a design procedure proposed to aid in the selection of PT reinforcement area and HBE sizing to prevent in-span plastic hinging, to force the maximum HBE moment to be at its ends, to keep PT reinforcement elastic, to select an adequate initial PT force, to account for moment/axial/shear interaction, and to account for PT losses due to axial shortening. Using this fundamental behavior knowledge, and adding response-based performance objectives to the above fundamental aspects of design, the companion paper investigates the seismic response of archetype SC-SPSWs using time-history nonlinear analyses.

Basic Principles of Self-Centering SPSW Systems

Fig. 1(a) shows the FBD of a SC-SPSW frame, where HBE is the horizontal boundary element, VBE is the vertical boundary element, P_{PT} is the PT axial compression force applied to the HBE, V_i is the externally applied lateral forces at story i due to applied seismic forces, and ω is the diagonal tension yield force of the web plate. The diagonal tension yield forces of the web plate can be resolved into vertical and horizontal components on the VBE and HBE as provided in Eqs. (1) and (2) (Sabelli and Bruneau 2007; Berman and Bruneau 2008), respectively

$$\omega_{cx} = F_{yp}t(\sin \alpha)^2 \quad \omega_{cy} = \frac{F_{yp}t \sin 2\alpha}{2} \quad (1)$$

$$\omega_{bx} = \frac{F_{yp}t \sin 2\alpha}{2} \quad \omega_{by} = F_{yp}t(\cos \alpha)^2 \quad (2)$$

where F_{yp} and t = yield stress and thickness of the web plate, respectively, and α = angle of inclination of the diagonal tension field from the vertical axis, as typically calculated for SPSWs (AISC 2005). Here, forces shown on the FBD are taken assuming that the web plate thickness varies proportional to increasing story shears.

A SC-SPSW differs from a conventional SPSW in that HBE-to-VBE rigid moment connections in a conventional SPSW are replaced by PT rocking moment connections. This allows a joint gap opening to form between the VBE and HBE interface about a rocking point, leading to a PT elongation, which is the self-centering mechanism [shown schematically in Fig. 1(b)]. One

possible rocking detail connection is shown in Fig. 1(c). The PT boundary frame is designed to essentially remain elastic, and hysteretic energy dissipation is intended to be provided by the web plate only.

The total hysteretic response of a SC-SPSW is provided by the combined elastic response of the PT boundary frame and the inelastic energy dissipation of the web plate. Similarly to self-centering moment frames (see previous cited references), the PT boundary frame response loads and unloads along a bilinear elastic force-displacement curve; the initial frame stiffness is provided by the PT joint connection, up to the point of joint opening that defines the “decompression” moment. Once the decompression moment is exceeded, the PT boundary frame follows a second force-displacement path of lower lateral frame stiffness, dependent on the interaction of the axial stiffness of the PT and the boundary beam (see Clayton et al. 2012). It is this bilinear elastic response of the PT boundary frame when combined with the inelastic hysteretic response of the energy dissipation elements that provides the characteristic “flag-shaped” hysteretic response of self-centering lateral force-resisting systems. For a SC-SPSW system, the idealized cyclic hysteretic response assuming a rigid boundary frame and an elastic-perfectly-plastic hysteretic model of the web plate is shown in Fig. 2. To better understand the behavior of a SC-SPSW system, the moment, shear, and axial force diagrams for the HBE are developed based on first principles.

Free-Body-Force Diagram

Fig. 3 shows the general FBD of HBE and VBE elements located at an intermediate floor level of a SC-SPSW frame once the web plate has fully yielded, where W_{bx1} , W_{bx2} and W_{by1} , W_{by2} are, respectively, the horizontal and vertical force resultants along the length of the HBE; W_{cx1} , W_{cx2} and W_{cy1} , W_{cy2} are, respectively, the horizontal and vertical force resultants along the height of the VBE; subscripts 1 and 2, respectively, denote the level below and above the HBE (here assuming that the force components labeled with subscript 1 are larger than subscript 2 associated with a thicker web plate below the HBE than above); h is the story height; and all other terms have been defined previously. Note that the vertical HBE end reactions would have to be resisted by a shear tab connection to the VBE (or equivalent); however, for clarity, the

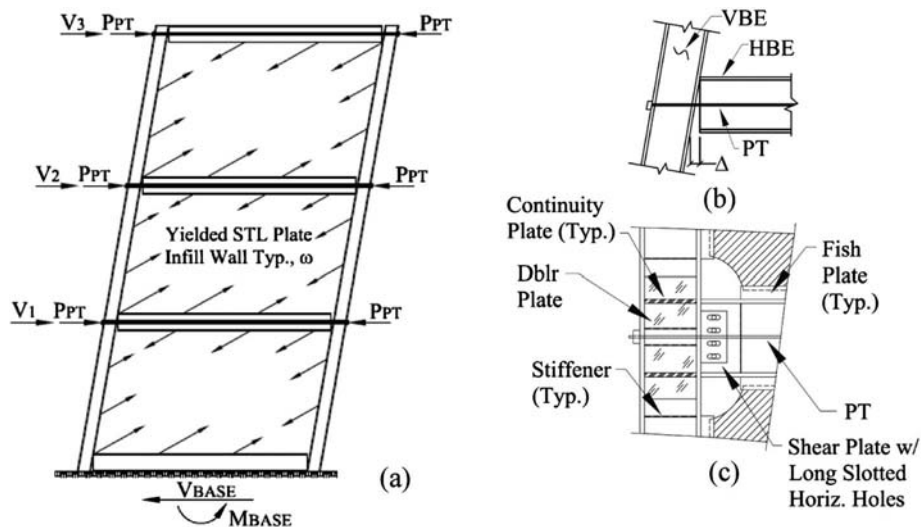


Fig. 1. SC-SPSW: (a) yield mechanism self-centering SPSW; (b) rocking joint; (c) rocking detail

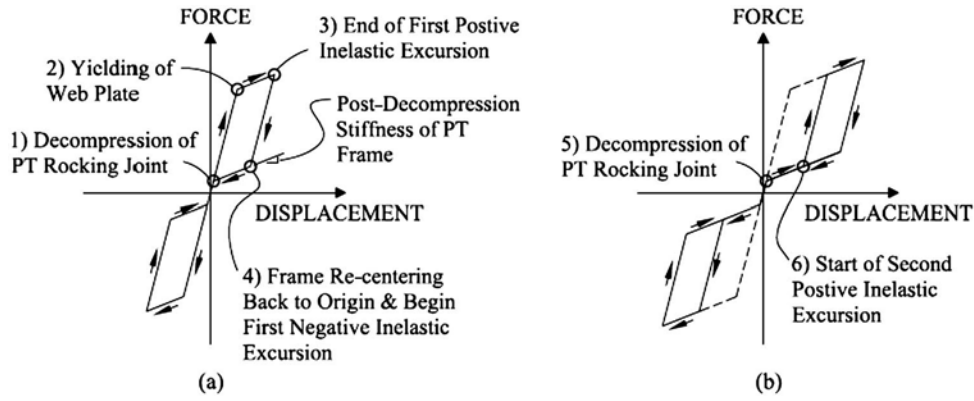


Fig. 2. Idealized hysteretic response of sc-spsw: (a) cycle 1; (b) cycle 2

shear tab is not shown in the FBD illustrated. The above force resultants are next separated into individual components such that their influence on the HBE can be more clearly understood.

First, Fig. 4 shows that the vertical components of the yielded web plate forces acting on the HBE above and below the HBE produces net vertical forces along the length of the HBE and vertical end reactions at the ends of the HBE equal to

$$R_1 = \frac{W_{by1} - W_{by2}}{2} \quad (3)$$

As shown in Fig. 4, L is the HBE span length, and R is the length of the web plate corner cutout at each end of the HBE provided to accommodate the HBE-to-VBE joint rocking connection detailing and to reduce the potential for corner tearout of the web plate due to high localized web plate strain effects during opening of the rocking joint connection.

The horizontal component of the yielded web plate forces acting along the length of the HBE, W_{bx1} and W_{bx2} , are shown in Fig. 5. In Fig. 5, d is the depth of the HBE, R_2 is the reaction force to maintain equilibrium, and all other terms have been defined previously. Here, assuming that the seismic story shear at each level, $V_{webplate}$, is distributed equally at each end of the HBE and that any vertical reaction due to unbalanced loading from $V_{webplate}$ is negligible, equilibrium gives

$$V_{webplate} = W_{bx1} - W_{bx2} \quad (4)$$

Replacing the resultant forces by the equivalent force per unit length quantities from Eq. (2) gives

$$\begin{aligned} V_{webplate} &= (\omega_{bx1} - \omega_{bx2})(L - 2R) \\ &= \frac{1}{2}(t_1 - t_2)F_{yp}(L - 2R) \sin(2\alpha) \end{aligned} \quad (5)$$

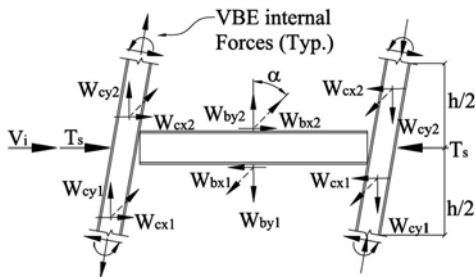


Fig. 3. Resultant force FBD

where t_1 and t_2 are the web plate thicknesses below and above the HBE, respectively, and all other terms have been defined previously. Eq. (5) represents the portion of the total base shear contribution provided by the web plate only. Assuming a rigid boundary frame and pinned support fixities at the VBE base, the ultimate lateral strength of the PT boundary frame contribution can be estimated based on energy principles (Berman and Bruneau 2003) leading to

$$\sum_{i=1}^{n_s} V_{frame,i} h_i = \sum_{i=1}^{n_s} M_{Conn,i} \quad (6)$$

where $V_{frame,i}$ is the lateral force at level i (based on a first-mode distribution defined in ASCE 07-10 or any other base shear distribution deemed by the engineer), h_i is the i th story elevation, n_s is the total number of stories, and $M_{conn,i}$ is the PT rocking moment connection strength at each beam level and for each connection is

$$M_{Conn} = T_s \left(\frac{d}{2} \right) \quad (7)$$

where T_s is defined in Eq. (17) and all other terms have been defined previously. Note that the use of Eq. (6) to calculate V_{frame} assumes that the VBEs (and diaphragm) do not provide restraint to beam growth (Christopoulos 2002; Garlock 2003); strategies have been proposed to design diaphragms to accommodate beam growth (Garlock 2008), but VBE flexibility is required in multi-story frames for the same purpose (Kim and Christopoulos 2009). The total base shear demand can then be approximated as

$$V_{BaseShear} = \sum_{i=1}^{n_s} (V_{webplate,i} + V_{frame,i}) \quad (8)$$

For the case of a single-story, single-bay SC-SPSW, VBE restraint to beam growth does not occur. The ultimate base shear demand, where all parameters have been defined previously, then becomes without approximation

$$V_{BaseShear(SingleStory)} = \frac{1}{2}(t)F_{yp}(L - 2R) \sin(2\alpha) + T_s \left(\frac{d}{h} \right) \quad (9)$$

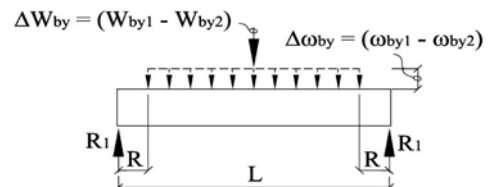


Fig. 4. FBD vertical component

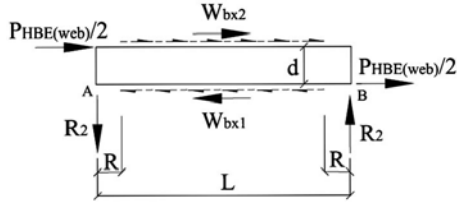


Fig. 5. FBD horizontal component along HBE

Note that, here, $V_{webplate}$ is equivalent to $P_{HBE(web)}$ in the *AISC Design Guide 20* (Sabelli and Bruneau 2007) for conventional SPSW systems, and this notation is used hereinafter. The vertical reaction at the ends of the HBE, R_2 , obtained by summation of moments about point B , is

$$R_2 = \frac{P_{HBE(web)}}{2} \left(\frac{d}{L} \right) + W_{bx2} \left(\frac{d}{L} \right) = (W_{bx2} + W_{bx1}) \left(\frac{d}{2L} \right) \quad (10)$$

Note that, in Fig. 5, if no corner cutout is provided (i.e., $R = 0$), then the couples formed by the reaction R_2 and the horizontal forces along the length of the HBE balance out such that no moment is induced along the HBE. In this special case, the moment induced to the HBE is the unbalanced moment from the story shear force (i.e., $P_{HBE(web)}/2$) applied at the rocking point.

Fig. 6 shows the horizontal components that produce reactions at the rocking points from force components developed outside of the HBE, due to yielding of the web plate (i.e., $W_{cx1} + W_{cx2}$) along the height of the VBE and due to the PT element anchored to the outside of the VBE flange (i.e., T_s). In keeping with the terminology used in the *AISC design guide*, ($W_{cx1} + W_{cx2}$) here is equivalent to $P_{HBE(VBE)}$. Fig. 6 reveals that the eccentricity between the horizontal rocking reactions produces a force couple resisted by the couple of vertical reactions at the ends of the HBE, equal to

$$R_3 = (T_s + P_{HBE(VBE)}) \left(\frac{d}{L} \right) = (T_s + W_{cx1} + W_{cx2}) \left(\frac{d}{L} \right) \quad (11)$$

For the PT element component, T_s in Eq. (11) consists of an initial PT force, T_o , applied at the time of construction of the SPSW system and which remains for the life of the building structure (minus long-term stress losses if applicable), and an incremental force, ΔT , due to PT elongation when the building drifts and the SPSW joint connections open due to rocking action at the HBE-to-VBE joints during an earthquake. The drift induced elongation of the PT elements at the HBE-to-VBE joint connection, producing the incremental force ΔT , for the condition of the PT reinforcement distributed symmetrically about the HBE neutral axis, where d is the depth of the HBE and ϕ_{drift} is the relative HBE-to-VBE joint rotation and is calculated as

$$\Delta_{drift} = 2 \left(\phi_{drift} \frac{d}{2} \right) = \phi_{drift} d \quad (12)$$

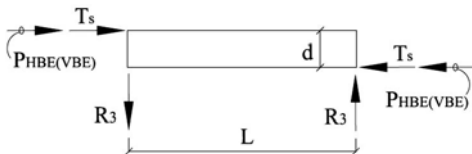


Fig. 6. FBD horizontal component outside HBE

Note that the axial loads generated on the HBE can be substantial and stress losses due to PT relaxation should also be considered when designing the posttensioning elements of the SC-SPSW system. As such, equilibrium of axial forces requires that the increase in tension forces in the PT elements equals the increase in compressive forces on the HBE (Garlock 2003). For SC-SPSW systems, for equal story force equally distributed at each end of the HBE, the PT force losses are attributed to the HBE axial shortening under the axial compression force from the VBE and the axial compression force due to the PT elongation during lateral drift. The corresponding axial shortening of the HBE is

$$\Delta_{loss} = \frac{P_{PT} L_{HBE}}{A_{HBE} E_{HBE}} + \frac{P_{HBE(VBE)} L_{HBE}}{A_{HBE} E_{HBE}} = \frac{P_{PT}}{k_{HBE}} + \frac{P_{HBE(VBE)}}{k_{HBE}} \quad (13)$$

where L_{HBE} = length of the HBE; L_{PT} = length of the PT elements; A_{HBE} = cross-sectional area of the HBE; A_{PT} = area of PT; E_{HBE} and E_{PT} = moduli of elasticity of the HBE and PT, respectively; k_{HBE} = axial stiffness of the HBE; P_{PT} = axial compression force on the HBE from the PT elements; and $P_{HBE(VBE)}$ = axial compression force on the HBE from the VBE. Solving Eq. (13) for P_{PT} leads to the following

$$P_{PT} = k_{HBE} \Delta_{loss} - P_{HBE(VBE)} \quad (14)$$

Accordingly, the net effective axial tension force in the PT elements is the elongation due to drift minus the axial shortening of the HBE and is calculated as follows

$$T_{PT} = \left(\frac{A_{PT} E_{PT}}{L_{PT}} \right) (\Delta_{drift} - \Delta_{loss}) = k_{PT} (\Delta_{drift} - \Delta_{loss}) \quad (15)$$

Equating Eqs. (14) and (15) such that $P_{PT} = T_{PT}$ and solving for Δ_{loss} leads to

$$\Delta_{loss} = \frac{P_{HBE(VBE)}}{k_b + k_{PT}} + \left(\frac{k_{PT}}{k_b + k_{PT}} \right) \Delta_{drift} \quad (16)$$

The resulting equation for T_s , which includes losses due to HBE axial shortening, is

$$T_s = T_o + \Delta T = T_o + \frac{A_{PT} E_{PT}}{L_{PT}} (\Delta_{drift} - \Delta_{loss}) \quad (17)$$

Superimposing all of the above force components identified to be acting on the HBE element, Fig. 7 shows the resulting FBD of an HBE for the condition when the web plate above and below the HBE flanges have fully yielded (for a rightward drift condition). To simplify the FBD shown, the horizontal compression reaction at the rocking connection at the left end of the HBE are combined

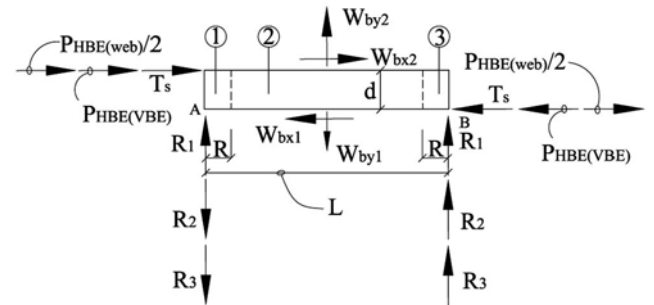


Fig. 7. Complete force resultant FBD of HBE

into a single variable C and is a maximum value for a rightward drift, which in terms of force resultants is

$$C = \frac{P_{\text{HBE(web)}}}{2} + P_{\text{HBE(VBE)}} + T_s \quad (18)$$

Additionally, the vertical end shear components have been combined and designated as reaction R_a and R_b for the left and right end vertical reactions, respectively. Substituting Eqs. (3), (10), and (11) results in the following equations in terms of force resultants:

$$\begin{aligned} R_a &= R_1 - R_2 - R_3 \\ &= \frac{W_{by1} - W_{by2}}{2} - (W_{bx1} + W_{bx2}) \frac{d}{2L} - (T_s + W_{cx1} + W_{cx2}) \frac{d}{L} \end{aligned} \quad (19)$$

$$\begin{aligned} R_b &= R_1 + R_2 + R_3 \\ &= \frac{W_{by1} + W_{by2}}{2} + (W_{bx1} + W_{bx2}) \frac{d}{2L} + (T_s + W_{cx1} + W_{cx2}) \frac{d}{L} \end{aligned} \quad (20)$$

Note that although the vertical gravity loads that may be present are not considered here, they could easily be incorporated in the analysis presented above. Also, the above formulations developed consider only a single-story PT frame contribution. For use with multistory frames, the additional lateral story shear force at each HBE level due to multistory PT frame stiffness (i.e., VBE's fighting beam growth) would have to be considered for preciseness in calculating the HBE demands (Kim and Christopoulos 2009).

Development of HBE Moments

The moment distribution to be used in the design of an HBE incorporating self-centering components can be determined from the FBD of Fig. 7. Three zones along the HBE are considered: the two segments of HBE where the web plate is cut out and not in contact with the HBE flange (Zones 1 and 3) and the segment of the HBE between the web plate corner cut outs where the web plate is in contact with the HBE flange (Zone 2), as shown in Fig. 7. Taking moment equilibrium at various locations along the HBE at each zone gives, in terms of force resultants

$$M_1 = \frac{Cd}{2} + R_a x \quad (21)$$

$$M_2 = R_a x + C \frac{d}{2} + (W_{by2} - W_{by1}) \left(\frac{x - R}{2} \right) + (W_{bx2} + W_{bx1}) \frac{d}{2} \quad (22)$$

$$M_3 = R_a x + C \frac{d}{2} + (W_{by2} - W_{by1}) \left(x - \frac{L}{2} \right) + (W_{bx2} + W_{bx1}) \frac{d}{2} \quad (23)$$

where x is any distance along the HBE from point A shown in Fig. 7, and the radius, R , is projected from the end of the HBE. Note that if $R = 0$, only the equations for Zone 2 are needed. Substituting Eqs. (18) and (19) and the equivalent force per unit length quantities defined previously

$$\begin{aligned} M_1 &= T_s \left(\frac{d}{2} - \frac{d}{L} x \right) + (\omega_{by1} - \omega_{by2}) \left(\frac{L}{2} x - Rx \right) \\ &\quad + (\omega_{bx1} + \omega_{bx2}) \left(\frac{dR}{L} x - \frac{d}{2} x \right) \\ &\quad + (\omega_{cx1} + \omega_{cx2}) \left(\frac{d^2}{2L} x + \frac{dR}{L} x + \frac{dh}{4} - \frac{dh}{2L} x - \frac{d^2}{4} - \frac{dR}{2} \right) \\ &\quad + (\omega_{bx1} - \omega_{bx2}) \left(\frac{dL}{4} - \frac{dR}{2} \right) \end{aligned} \quad (24)$$

$$\begin{aligned} M_2 &= T_s \left(\frac{d}{2} - \frac{d}{L} x \right) + (\omega_{by1} - \omega_{by2}) \left(\frac{L}{2} x - \frac{x^2}{2} - \frac{R^2}{2} \right) \\ &\quad + (\omega_{bx1} + \omega_{bx2}) \left(\frac{dR}{L} x - \frac{dR}{2} \right) \\ &\quad + (\omega_{cx1} + \omega_{cx2}) \left(\frac{dR}{L} x + \frac{dh}{4} + \frac{d^2}{2L} x - \frac{dh}{2L} x - \frac{d^2}{4} - \frac{dR}{2} \right) \\ &\quad + (\omega_{bx1} - \omega_{bx2}) \left(\frac{dL}{4} - \frac{dR}{2} \right) \end{aligned} \quad (25)$$

$$\begin{aligned} M_3 &= T_s \left(\frac{d}{2} - \frac{d}{L} x \right) + (\omega_{by1} - \omega_{by2}) \left(\frac{L^2}{2} - LR - \frac{L}{2} x + Rx \right) \\ &\quad + (\omega_{bx1} + \omega_{bx2}) \left(\frac{dR}{L} x + \frac{dL}{2} - dR - \frac{d}{2} x \right) \\ &\quad + (\omega_{cx1} + \omega_{cx2}) \left(\frac{dR}{L} x + \frac{dh}{4} + \frac{d^2}{2L} x - \frac{dh}{2L} x - \frac{d^2}{4} - \frac{dR}{2} \right) \\ &\quad + (\omega_{bx1} - \omega_{bx2}) \left(\frac{dL}{4} - \frac{dR}{2} \right) \end{aligned} \quad (26)$$

It is instructive to plot the moment distribution along the length of an HBE for a SC-SPSW frame. For illustrative purposes only, to avoid abstract complexities in keeping the problem parametric, all results here are presented in terms of an example. This example considers a $W18 \times$ HBE with a clear span of 5.74 m (226 in.) and a story height of 3.89 m (153 in.) of a single-bay frame. The SPSW web plates consist of 14-gauge (1.83-mm) and 18-gauge (1.77-mm) thicknesses below and above the HBE, respectively, with a corner cut-out radius of 254 mm (10 in.). The area of PT steel was arbitrarily chosen to produce a maximum moment of 60% of the full HBE plastic moment capacity at the end span of the HBE for a 2% lateral drift (different drift magnitudes are recommended later for this purpose), with a T_o of 30% of the assumed yield strength of the PT. A yield stress of 207 MPa (30 ksi) was assumed for the web plates, an ultimate yield stress of 1,034 MPa (150 ksi) was assumed for the PT reinforcement, and ASTM A572 ($F_y = 345$ MPa) steel was used for the boundary frame. The moment equations above each are composed of five components, and each of the individual moment contributions are plotted in Fig. 8. It is observed from the moment diagrams that the horizontal reactions at the rocking point will always generate double curvature moments at the ends of the HBE. Additionally, the moment diagrams are of identical shape; only the moment magnitudes are different. Generally, the contribution of the moment due to the effects of the VBE being pulled toward each other by the yielding of the web plate is not as significant as the HBE moment produced by the applied PT force. The contribution to the HBE moment from the VBE horizontal reaction at the rocking point will always be additive to the HBE moment produced by the PT component. For comparison, the composite HBE moment diagram is plotted with and without the PT component in Fig. 9. Without the PT, it can be seen that the maximum moment occurs close

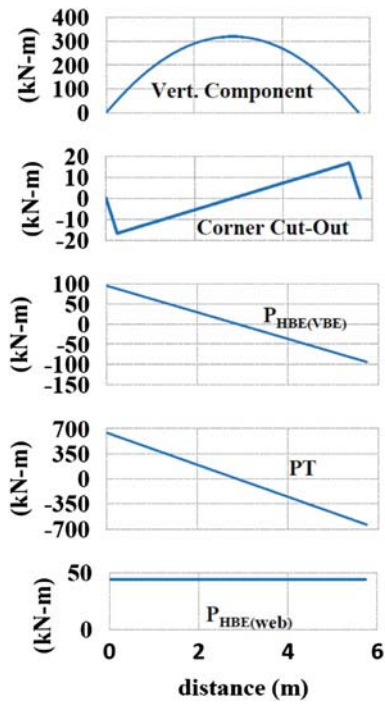


Fig. 8. HBE moment components

to the HBE mid span, which is not desirable for reasons described later. Therefore, in addition to acting as a self-centering mechanism, the PT forces can be designed to shift the point of maximum moment toward the ends of the HBE (although at the cost of increased HBE moment demand); additional discussion on this is presented later.

Development of HBE Shears and Axial Forces

The shear distribution to be used in the design of an HBE incorporating self-centering components can be determined using the same free-body diagrams developed earlier for the HBE moments. As a result, for the same three zones defined previously

$$V_1 = R_a = \frac{(\omega_{by1} - \omega_{by2})(L - 2R)}{2} - \frac{(\omega_{bx2} + \omega_{bx1})(L - 2R)}{2L}d - (\omega_{cx1} + \omega_{cx2})\left(\frac{h}{2} + \frac{d}{2} - R\right)\left(\frac{d}{L}\right) - T_s\left(\frac{d}{L}\right) \quad (27)$$

$$V_2 = R_a - (\omega_{by1} - \omega_{by2})(x - R) \quad (28)$$

$$V_3 = R_a - (\omega_{by1} - \omega_{by2})(L - 2R) \quad (29)$$

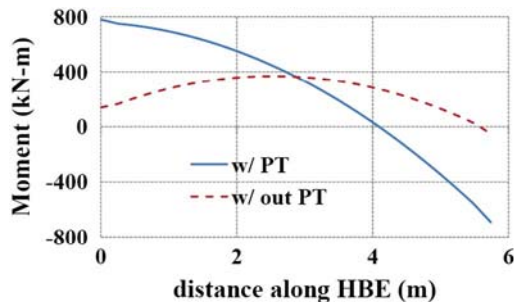


Fig. 9. Composite moment diagram

Similarly, for axial forces over each of the three zones

$$P_1 = C = \frac{(\omega_{bx1} - \omega_{bx2})(L - 2R)}{2} + (\omega_{cx1} + \omega_{cx2})\left(\frac{h}{2} - \frac{d}{2} - R\right) + T_s \quad (30)$$

$$P_2 = C - (\omega_{bx1} - \omega_{bx2})(x - R) \quad (31)$$

$$P_3 = C - (\omega_{bx1} - \omega_{bx2})(L - 2R) \quad (32)$$

Note that the development of the HBE moment, shear, and axial force formulations presented are based on a capacity design approach where the web plates have fully yielded. Consideration of HBE axial stiffness has been considered. For a precise representation of the effects of in-plane beam flexibility stiffness, a computer analysis would be needed. However, due to the inherent necessity that the boundary frame is designed to remain elastic, the HBE will, by design, be quite stiff and can, without significant loss in analysis results, be approximated as rigid for the purpose of neglecting the effects of the in-plane beam flexibility, as will be observed in the following section.

Comparison with Push-Over Analysis Results

To verify the formulations describing the distribution of moment, shear, and axial forces developed, comparisons were made to cyclic nonlinear push-over analysis using the computer program SAP2000 (CSI 2009). A strip model approach was used for the analytical modeling of the SPSW web plate (Sabelli and Bruneau 2007). Each of the strips was assigned an axial plastic hinge to model the nonlinear hysteretic behavior assuming an elastic-perfectly-plastic response. The PT elements along the length of the HBE were modeled as tension-only members, and temperature loading was used to simulate initial posttensioning forces, which allowed modeling the PT elements using simple frame elements. The VBE frame members were considered to be rigid. The rocking connection was modeled using Gap Link elements. Adopting similar methods used by Christopoulos (2002), a rigid frame element was used to model the depth of the HBE to capture the rocking motion about the HBE flanges, and the use of nodal constraints was used to transfer shear from the HBE-to-VBE connection. The analytical model is shown in Fig. 10.

For this example, a single-bay, single-story frame with a bay width of 6.1 m (20 ft) and story height of 3.05 m (10 ft) with material strengths and boundary frame members, as defined in the first example, is used. The SPSW web is a 14-gauge web plate (1.83 mm). A PT area of 3,290 mm² (5.1 sq. in.) is provided, at a T_o of approximately 25% of the assumed yield strength of the PT. Additionally, it is assumed that the boundary frame remains elastic. A comparison of the moment, shear, and axial force distributions along the length of the HBE using the above closed-form equations with the results obtained from the SAP2000 analysis is provided in Fig. 11 for a rightward 3% drift condition. Because of the finite number of strips to represent the web plate, the shear and axial force diagrams obtained from the computer model are stepped compared to the continuous force diagrams using the theoretical formulations. All results are in good agreement.

The hysteretic response from the cyclic nonlinear SAP2000 analysis is provided in Fig. 12 for both the rigid and flexible HBE frame conditions. For the rigid HBE, all the tension strips yield simultaneously leading to bilinear-shape hysteretic curves, whereas for the flexible HBE, progression in yielding of the tension

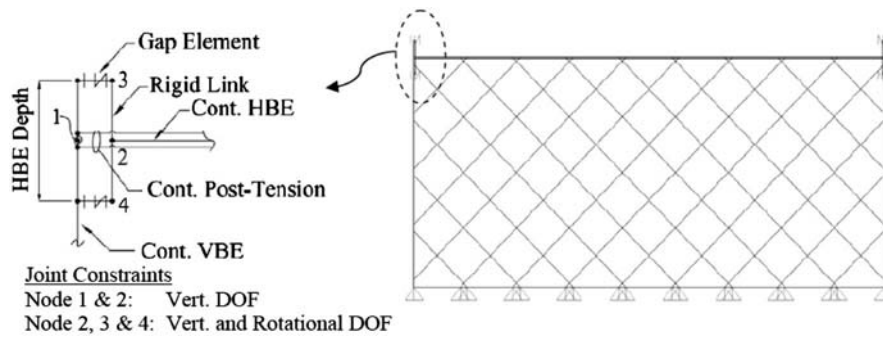


Fig. 10. SAP2000 model

strips leads to stepwise-shape hysteretic curves. Recentering is achieved in both cases.

Design Consideration of Self-Centering Connection

The above understanding of behavior and closed-form solutions also serve to instruct design, in particular to aid in the selection of PT reinforcement area and HBE sizing to prevent in-span plastic hinging, to force the maximum HBE moment to be at its ends, to keep PT reinforcement elastic, to select an adequate initial PT force, to account for moment-axial-shear interaction, and to account for PT losses due to HBE axial shortening. To illustrate these key design considerations, a prototype frame (Vargas and Bruneau 2006) is designed as a conventional 3-story SPSW in compliance with AISC 341 (AISC 2005) and is used as a starting point. Its top and bottom HBEs were $W18 \times 119$ and $W18 \times 130$, whereas $W18 \times 106$ and $W14 \times 132$ were used for intermediate HBEs and VBEs, respectively, with a story dimension of 6,096 mm (240 in.) \times 3,962 mm (156 in.). The web plates consisted of 13 gauges (2.28 mm), 14 gauges (1.82 mm), and 18 gauges (1.13 mm) for the first to the third story, respectively. Material strengths are the same as defined in the first example. To obtain a SC-SPSW, the rigid HBE-to-VBE connections were replaced by self-centering connections having, in this case, three layers of PT rods. For the current purpose, the HBE and VBE sections

were kept the same as for the conventional. This will be revisited when optimization issues are addressed later.

Moment Distribution on HBE with Self-Centering Connection

Fig. 13 presents normalized moment distributions along the intermediate HBE for different levels of PT forces normalized by the HBE plastic moment strength when the SC-SPSW yield mechanism has occurred. When no PT force is applied in the structure, maximum moment occurs close to mid span of the beam. In that case, moments at the HBE ends are caused by the compression forces coming from the VBEs, which squeeze the HBE and is applied through the contact points on the flanges during rocking. As the PT force applied to the structure increases, the HBE behaves progressively more like a fixed moment connection with higher end-moments. In addition, the location of the maximum moment (Fig. 13, diamond) also shifts, from close to the mid span toward the HBE ends.

Recognizing this behavior, one might question what level of PT forces is desirable when applied to a self-centering connection. Many feasible approaches are possible. For example, one might be tempted to apply PT forces such that they would create HBE end-moments at least identical to those that would have developed in the corresponding full rigid connection. In this example, this would require a PT force $T_s = 1,019$ kip (4,531 kN). However, this objective is actually misleading. First, the actual moment capacity of the HBE significantly reduces as the PT increase, which the normalized moment distribution in Fig. 13 does not capture; this will be addressed in a later section. Second, substantial reinforcement at the HBE ends would be required to resist such a large force applied to only one flange. Here, it is proposed instead to design for the smallest PT force needed to shift the point of maximum moment to occur at the HBE ends. In this design example, the PT force T_s is 354 kip (1,575 kN) and would create a maximum

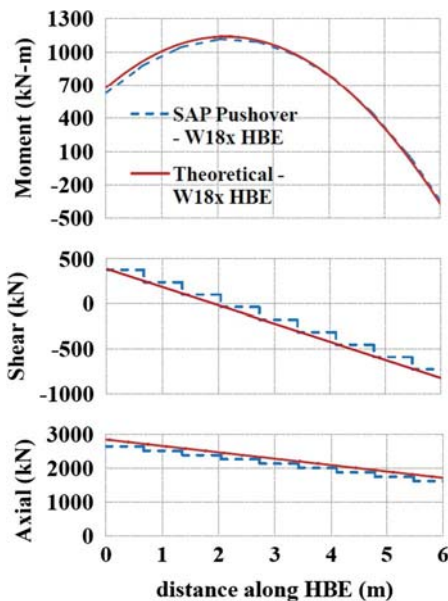


Fig. 11. SAP2000 push-over comparison

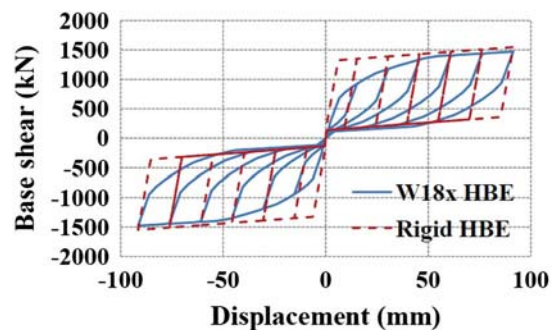


Fig. 12. SAP2000 hysteresis (3% drift)

moment in the connection of $0.4\phi M_p$. The advantages of selecting the smallest T_y such that the maximum moment occurs at the end of the HBE will become clearer in the subsequent sections.

Initial Posttension and Target Drift

As shown in Eq. (17), the total PT force T_y is the sum of an initial PT force T_0 and the additional forces ΔT generated by the rods (or strands) as they elongate. Unlike the initial PT force, the ΔT forces linearly increase as the relative rotation between the HBE and the VBE increases. Hence, one should recognize that the moment distribution plotted in Fig. 13 will vary depending on the magnitude of drift. One could reasonably question at what level of drift a specific moment distribution would be achieved and how much PT forces should be imposed initially on the rods (T_0).

To investigate these issues, using Eq. (17), the impact of total PT force on the HBE for different levels of initial PT forces (i.e., $0.4, 0.3, 0.2$, and $0.1T_y$) is examined. For the connection configuration considered in this study, if T_0 applied to the connection is equal to 0.3 and $0.4T_y$, the rods will yield at average drifts of 4.2 and 3.6% , respectively ($T_y = 0.85T_{pu}$, where T_y and T_{pu} = total yield strength and the ultimate tensile strength of the PT rods used). At a lower initial PT force (i.e., $\leq 0.2T_y$), the rods will not yield up to 4.8% drift. Hence, the higher the initial PT force imposed on the connection, the sooner the rods will yield as drift increases.

Experimental investigations of conventional SPSWs have reported that these structures performed well up to 3 or 4% drift under cyclic push-over loads (e.g., Driver et al. 1997; Behbahani et al. 2003; Vian and Bruneau 2005; Park et al. 2007; Qu et al. 2008). Therefore, for SC-SPSW to have a comparable performance, it is proposed here that the PT rods be designed to remain elastic at least up to 4% drift. If the PT rods undergo plastic deformation, the SC-SPSW might lose its self-centering capability. To satisfy this design requirement in this example, T_0 should be less than $0.3T_y$. In addition to the above requirement, it is proposed that SC-SPSW be designed such that the total PT force that shifts the point of maximum moment to the HBE ends is reached at the target drift. This is proposed to avoid the formation of plastic hinge along the HBE span. As reported by Purba and Bruneau (2010), development of in-span plastic hinges on HBE has detrimental impacts on the behavior of SPSW, with significant accumulation of plastic deformations on HBE and lower than expected lateral load resistance. Moreover, based on experimental observations, conventional SPSWs would be expected to reach approximately 2.5% drift during earthquakes, having a return period of 2,500 years (Qu et al. 2008). It is also a common practice in earthquake engineering to limit the drift of structures to 2% drift during design to ensure

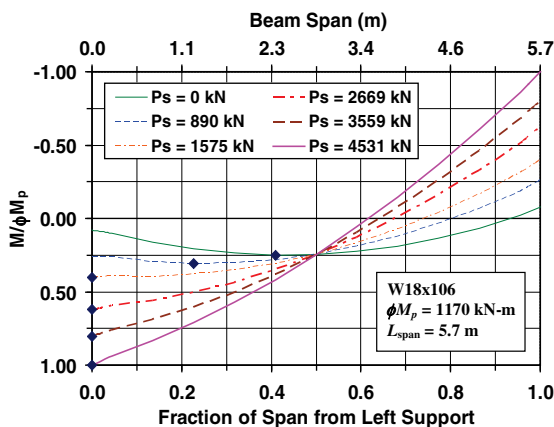


Fig. 13. Moment distribution on beam with self-centering connection

that they perform well under the design earthquake loads. However, using a target drift of 4% may be more consistent with the above requirement of PT remaining elastic at least up to 4% drift. For the current examples, a 2% target drift was arbitrarily chosen. However, larger target values may be required for SC-SPSW if demonstrated to be so required by analyses.

To help better assess the latter design consideration, Fig. 14 is prepared. In Fig. 14 normalized maximum moment is plotted as a function of drift for the initial PT levels of 0.2 and $0.3T_y$, respectively. Note that the $0.4T_y$ case would not satisfy the previous design requirement of elastic behavior of rods at 4% drift. In Fig. 14, five curves are plotted representing five different total cross-section areas of the rods as a percentage of the total beam cross-section areas. These curves are for the number of rods and geometry described previously. Results would be slightly different for different connection geometry. In both cases, the moment at 0% drift is defined as the “decompression moment,” the moment that must be exceeded prior to joint opening of the rocking connection and can be calculated as

$$M_{\text{decomp}} = T_0 \frac{d}{2} \quad (33)$$

where all terms have been defined previously. As a minimum, one should design T_0 such that the resulting decompression moment would be sufficient to resist the end-moments induced by the gravity loads. Some level of resistance to wind loads may also be desirable without decompression.

Beyond the web plate yielding point (i.e., beyond 0.3% drift), each normalized maximum moment curve actually first consists of a quadratic-shaped segment, followed by a linearly increasing one. The quadratic part of the curve indicates that the location of maximum moment is somewhere within the HBE span. In this case, the

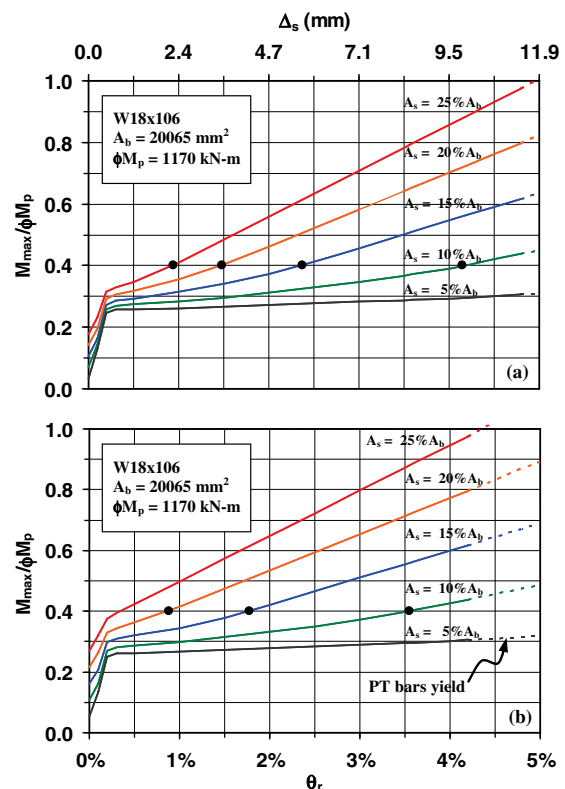


Fig. 14. Normalized maximum moment as a function of drift: (a) $T_0 = 0.2T_y$; (b) $T_0 = 0.3T_y$

maximum moment is governed by the vertical component of tension force in the infill plate, and its effect outweighs the moment developed by the total PT force (see Fig. 8). On the linear part of the curve, this situation is reversed; the maximum moment is governed by the total PT force and occurs at the HBE ends. The point where these two segments meet (located in the figures by a circle) indicates when the maximum moment is reached at the HBE ends, which, in this particular self-centering connection, is $0.4\phi M_p$. Note that the curve for $A_s = 5\%A_b$ line in Fig. 14 does not contain any linear segment because the moment caused by the available total PT forces are much less compared to those caused by the vertical component of tension force in the web plate. On the other hand, there are some cases where the entire curve consists of linear segments (e.g., the $25\%A_b$ for $T_0 = 0.3T_y$). This indicates that the contribution to the moment diagram due to the imposed initial PT force outweighs the moment caused by other effects.

To design the example self-centering connection, if T_0 imposed in the connection is equal to $0.2T_y$ [i.e., Fig. 14(a) is used] and it is designed to reach the maximum moment at the end of the HBE at an arbitrarily chosen target drift of 2% ($M_{max} = 0.4\phi M_p$ based on the previous information), then one needs to provide a total PT cross-section area of 5.20 sq.in. = 3,410 mm² (i.e., $A_s = 17\%A_b$) by interpolation between the circular dots at 1.5 and 2.4% drift on the $A_s = 20\%A_b$ and $A_s = 15\%A_b$ lines, respectively, for the same level of maximum moment $0.4\phi M_p$. Alternatively, the same design requirement (i.e., $M_{max} = 0.4\phi M_p$ reached at target drift) can be achieved by imposing a higher initial PT (i.e., $T_0 = 0.3T_y$) and using a smaller total cross-section area of rods (i.e., 4.38 sq.in. = 2,825 mm² or $A_s = 14\%A_b$, obtained from the same interpolation process, this time on Fig. 14(b), between the circular dots at 1.8 and 3.6% drift on the $A_s = 15\%A_b$ and $A_s = 10\%A_b$ lines, respectively). From a cost perspective, taking the least possible cross-section area of rods to satisfy the aforementioned design requirement (assuming that all design choices have the same detailing cost), the latter design option is more desirable for this particular connection. Here, the initial PT forces and the total PT force at 2% drift are 0.3 and $0.63T_y$, respectively; the total cross-section areas of the rods needed are 14% of the HBE cross section; and the maximum moment at 2% drift is $0.4\phi M_p$ and occurs at the HBE ends. In addition, the rods remain elastic ($T_s = 0.97T_y$) at 4% drift, and the corresponding maximum moment at this point is approximately $0.57\phi M_p$.

Reduced Moment Capacity and Posttension Losses

Reduced plastic moment due to axial and shear forces ($M_{pr}^{P,V}$) can be estimated based on the procedure explained by Bruneau et al. (2011). For the example at hand, knowing that at 2% drift the HBE experiences compression forces of 1,971 kN (443 kip) and shear forces of 406 kN (92 kip), the plastic moment is reduced by 17% from its pure flexure value ($M_{pr}^{P,V} = 83\% \phi M_p = 973 \text{ kN}\cdot\text{m} = 718 \text{ kip}\cdot\text{ft}$). Note that the compression forces consist of 1,575 kN (354 kip) plus 396 kN (89 kip), respectively, caused by the PT rods and by the web plate forces on the VBEs that create a compression on the HBE ($T = T_s + W_{cx} = 0.28P_{yb}$). Since the HBE required only 40% of its pure flexure plastic moment at 2% drift ($M_d = 40\% \phi M_p = 468 \text{ kN}\cdot\text{m} = 345 \text{ kip}\cdot\text{ft}$, as mentioned previously), this would actually be 48% of $M_{pr}^{P,V}$. Note that this leaves the HBE with a 52% reserve capacity as excess strength, although at 4% drift the same HBE only has 17% reserve strength left. A graphical illustration of the relationship between target moment (M_{target}), reduced plastic moment due to axial and shear forces ($M_{pr}^{P,V}$), and level of PT force applied in the connection (T_s) is shown in Fig. 15.

Furthermore, as shown in Eq. (16), the amount of PT relaxation is caused by the axial shortening of the HBE due to (1) the axial compression load at the rocking point from the VBE horizontal reaction and (2) the axial compression load from the PT forces produced during lateral drift. After yielding of the web plate, the first component of losses becomes independent from the magnitude of drift, because the tension forces from the web plate remain constant, assuming the web plate behaves as a perfectly plastic material. Unlike the first losses component, the second losses component linearly increases as the magnitude of drift also increases. For the current example, at 2% drift, the elongation of the PT rods is 9.50 mm (3.74 in.) calculated using Eq. (12), and the axial shortening of the HBE due to the first and second components of Eq. (16) are 0.56 mm (0.22 in.) and 1.18 mm (0.46 in.), respectively. The results imply that the actual elongation is not 9.50 mm (3.74 in.) but only 7.75 mm (3.06 in.). Hence, the total PT force imposed in the condition is actually smaller than 1,575 kN (354 kip), and, as a consequence, the resulting moment in the HBE is also smaller than $0.4\phi M_p$. One possible solution to resolve this situation is increasing the total cross-section area of the rods such that the total PT forces after considering losses [per Eq. (17)] are back to 1,575 kN (354 kip). However, this requires an iterative process because increasing the area of the rods will also increase the losses [per Eq. (16)]. For example, iterating using these two equations to achieve a value of T_s equal to 1,575 kN (354 kip) at 2% drift, a revised total cross-section areas of rods of 3,155 mm² (4.89 sq.in.) is obtained (i.e., a 12% increase from the previous result).

Design Optimization of Self-Centering Connection

For the first step of this design example (although other approaches are possible and acceptable), the SC-SPSW was designed as if it was a conventional SPSW. Afterward, design requirements outlined in the previous sections were used to select PT forces. Recognizing that the HBE end-moments in the SC-SPSW would be less than in a conventional SPSW having full rigid connections, a smaller section can be used. An interactive design curve, as shown in Fig. 15, can be useful for this purpose. In Fig. 15, plotted on the x-axis is the normalized target moment; on the left and right y-axes are normalized reduced plastic moment and level of PT force, respectively. Using the previous results as an example [knowing that a PT force of 1,575 kN (354 kip) would create maximum moment on the HBE of $0.4\phi M_p$], a horizontal line is drawn at 354 kip starting from the right y-axis of Fig. 15 to intersect the

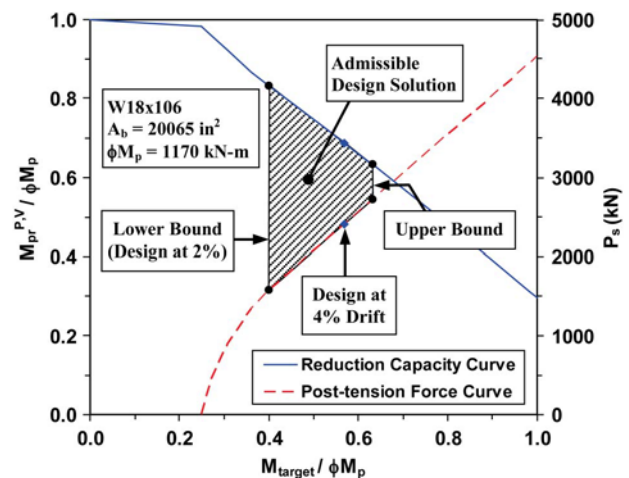


Fig. 15. Interaction curve for optimization of HBE section

“posttension force” curve (dashed line), from which a vertical line is drawn (at of $0.4\phi M_p$ from the x -axis). The intersection of the vertical line with the “reduction capacity” curve (Fig. 15, solid line) is used to find the reduced plastic moment corresponding to this particular PT force. For this example, the reduced HBE plastic moment due to axial and shear forces is $0.83\phi M_p$. This condition serves as the lower bound of the admissible design-solution zone (Fig. 15, shaded area). The upper bound of the zone is the condition for which the target moment (caused by $T_s = 2,719$ kN = 611 kip) is approximately equal to the actual moment capacity of the HBE (i.e., $M_{\text{target}} = M_{pr}^{P,V} = 0.63\phi M_p$). All designs that fall within this range delimited by the shaded area in Fig. 15 are deemed to be admissible solutions. Fig. 15 also allows to verify that the same HBE can resist moments corresponding to drifts up to 4% (which would correspond to a value of $T_s = 2,405$ kN = 541 kip, $M_{\text{target}} = 0.57\phi M_p$, and $M_{pr}^{P,V} = 0.69\phi M_p$) with 17% reserve strength left. This indicates that the HBE has a reserve capacity to resist a greater moment and that it could be optimized by choosing a smaller section. In addition, using Fig. 15, one can judge that selecting PT forces to create HBE end-moments nearly identical to those that would have developed in the corresponding full moment-resisting connection (i.e., close to ϕM_p) is impossible. For example, if a PT force of 4,003 kN (900 kip) was applied to the connection, it would create maximum moment on the HBE of $0.89\phi M_p$; however, because of the ensuing high axial force, the reduced plastic capacity of the HBE is only $0.4\phi M_p$, i.e., significantly less than needed to resist the resulting moment.

To optimize the HBE size used in the self-centering connection, a $W18 \times 97$ was selected. It’s interaction design curves (not shown) confirms that at 2% drift, the HBE requires 43% of its unreduced plastic moment and 54% of its plastic moment reduced due to compression and shear forces to resist the applied moment; although at 4% drift, the same HBE has no more reserve strength ($M_{\text{target}} \approx M_{pr}^{P,V}$).

Design Procedures of Self-Centering Connection

Building on the design example, system behavior, and performance objectives presented above, the following design procedure for SC-SPSW HBE-to-VBE connection is proposed. The design procedure presented here is applicable for any type of connection developing rocking about the HBE flanges.

1. Select initial boundary element sizes and web plate thickness (of many possible approaches, this could be done by designing a conventional SPSW, although other approaches are acceptable too).
2. Design the self-centering connection with the least PT forces that would result in the maximum moment occurring at the HBE ends at the target drift.
3. Select posttension to ensure that the PT rods remain elastic at least up to 4% drift.
4. Select the initial PT force applied to the self-centering connection to be also large enough to provide an adequate decompression moment to overcome gravity loads and possible wind loads.
5. Select the least cross-section areas of PT rods that satisfy the previous conditions.
6. Consider the effect of PT on reducing the HBE plastic moment as well as the effect of PT losses due to axial shortening to assess the adequacy of the HBE.
7. Iterate as needed to reduce the HBE size, ensuring that the HBE moment capacity reduced due to axial and shear forces remains adequate.

Conclusions

Fundamental behavior of a SC-SPSW was presented, in terms of closed-form equations for moment, shear, and axial forces along the HBE. These were verified by nonlinear cyclic push-over analysis. These formulations and development of the free-body diagrams presented not only provide insight on the behavior of a SC-SPSW system but also provide a means to inform design. On the basis of that knowledge, a proposed HBE and PT connection design procedure was formulated and illustrated by a design example. The findings presented indicate that SC-SPSW systems could be a viable alternative to traditional lateral force-resisting systems. Future research is needed to further validate this system, including experimental work to investigate its behavior and self-centering characteristics.

Acknowledgments

Support was provided in part by the National Science Foundation as part of the George E. Brown Network for Earthquake Engineering Simulation under award number CMMI-0830294. Any opinions, findings, and conclusions presented in this paper are those of the authors and do not necessarily reflect the views of the sponsors.

References

- American Institute of Steel Construction (AISC). (2005). “Seismic provisions for structural steel buildings.” *ANSI/AISC 341-05*, Chicago.
- Behbahanifard, M. R., Grondin, G. Y., and Elwi, A. E. (2003). “Experimental and numerical investigation of steel plate shear wall.” *Struct. Eng. Rep.* 254, Dept. of Civil Engineering, Univ. of Alberta, Edmonton, Alberta, Canada.
- Berman, J. W., and Bruneau, M. (2003). “Plastic analysis and design of steel plate shear walls.” *J. Struct. Eng.*, 129(11), 1448–1456.
- Berman, J., and Bruneau, M. (2008). “Capacity design of vertical boundary elements in steel plate shear walls.” *Am. Inst. Steel Constr. Eng. J.*, First Quarter, 57–71.
- Bruneau, M., Uang, C. M., and Sabelli, R. (2011). *Ductile design of steel structures*, 2nd Ed., McGraw-Hill, New York.
- Canadian Standards Association (CSA). (2009). “Design of steel structures.” *CAN/CSA-S16-09*, Willowdale, Ontario, Canada.
- Christopoulos, C. (2002). “Self-centering post-tensioned energy dissipating (PTED) steel frames for seismic regions.” Ph.D. thesis, Dept. of Structural Engineering, Univ. of California, San Diego, La Jolla, CA.
- Christopoulos, C., Filiatrault, A., and Folz, B. (2002a). “Seismic response of self-centering hysteretic SDOF systems.” *Earthquake Eng. Struct. Dyn.*, 31(5), 1131–1150.
- Christopoulos, C., Filiatrault, A., Uang, C. M., and Folz, B. (2002b). “Post-tensioned energy dissipating connections for moment-resisting steel frame.” *J. Struct. Eng.*, 128(9), 1111–1120.
- Clayton, P. M., Berman, J. W., and Lowes, L. N. (2012). “Seismic design and performance of self-centering steel plate shear walls.” *J. Struct. Eng.*, 138(1), 22–30.
- Driver, R. G., Kulak, G. L., Kennedy, D. J. L., and Elwi, A. E. (1997). “Seismic behavior of steel plate shear walls.” *Struct. Eng. Rep.* 215, Dept. of Civil Engineering, Univ. of Alberta, Edmonton, Alberta, Canada.
- Garlock, M. (2003). “Design, analysis, and experimental behavior of seismic resistant post-tensioned steel moment frames.” Ph.D. thesis, Dept. of Civil and Environmental Engineering, Lehigh Univ., Bethlehem, PA.
- Garlock, M., and Li, J. (2008). “Steel self-centering moment frames with collector beam floor diaphragms.” *J. Constr. Steel Res.*, 64(5), 526–538.
- Garlock, M., Ricles, J., and Sause, R. (2005). “Experimental studies of full-scale posttensioned steel connections.” *J. Struct. Eng.*, 131(3), 438–448.

- Kim, H.-J., and Christopoulos, C. (2009). "Seismic design procedure and seismic response of post-tensioned self-centering steel frames." *Earthquake Eng. Struct. Dyn.*, 38(3), 355–376.
- Park, H. G., Kwack, J. H., Jeon, S. W., Kim, W. K., and Choi, I. R. (2007). "Framed steel plate wall behavior under cyclic lateral loading." *J. Struct. Eng.*, 133(3), 378–388.
- Purba, R., and Bruneau, M. (2010). "Impact of horizontal boundary elements design on seismic behavior of steel plate shear walls." *Tech. Rep. MCEER-10-0007*, Multidisciplinary Center for Earthquake Engineering Research, State Univ. of New York at Buffalo, Buffalo, NY.
- Qu, B., Bruneau, M., Lin, C. H., and Tsai, K. C. (2008). "Testing of full scale two-story steel plate shear walls with reduced beam section connections and composite floors." *J. Struct. Eng.*, 134(3), 364–373.
- Ricles, J., Sause, R., Peng, S., and Lu, L. (2002). "Experimental evaluation of earthquake resistant posttensioned steel connections." *J. Struct. Eng.*, 128(7), 850–859.
- Rojas, P., Ricles, J., and Sause, R. (2005). "Seismic performance of post-tensioned steel moment resisting frames with friction devices." *J. Struct. Eng.*, 131(4), 529–540.
- Sabelli, R., and Bruneau, M. (2007). "Steel plate shear walls." *AISC Steel Design Guide 20*, American Institute of Steel Construction, Chicago.
- SAP2000 Version 14.1.0* [Computer software]. Computers and Structures (CSI), Berkeley, CA.
- Vargas, R., and Bruneau, M. (2006). "Experimental investigation of the structural fuse concept." *Tech. Rep. MCEER-06-0005*, Multidisciplinary Center for Earthquake Engineering Research, State Univ. of New York at Buffalo, Buffalo, NY.
- Vian, D., and Bruneau, M. (2005). "Steel plate shear walls for seismic design and retrofit of building structures." *Tech. Rep. No. MCEER-05-0010*, Multidisciplinary Center for Earthquake Engineering Research, State Univ. of New York at Buffalo, Buffalo, NY.